JACS
JOURNAL OF THE AMERICAN CHEMICAL SOCIETY
pubs.acs.org/JACS
Article

Conjugated Zwitterionic Oligomers as Ligands on Perovskite Nanocrystals: Hybrid Structures with Tunable Interparticle Spacing

Christopher Cueto, Mingqiu Hu, Thomas P. Russell, and Todd Emrick*

Cite This: J. Am. Chem. Soc. 2024, 146, 8189−8197
Read Online
ACCESS | Metrics & More | Article Recommendations | Supporting Information

ABSTRACT: Conventional ligands for $CsPbBr_3$ perovskite nanocrystals (NCs), composed of polar, coordinating head groups (e.g., ammonium or zwitterionic) and aliphatic tails, are instrumental in stabilizing the NCs against sintering and aggregation. Nonetheless, the aliphatic (insulating) nature of these ligands represents drawbacks with respect to objectives in optoelectronics, and yet removing these ligands typically leads to a loss of colloidal stability. In this paper, we describe the preparation of $CsPbBr_3$ NCs in the presence of discrete conjugated oligomers that were prepared by an iterative synthetic approach and capped at their chain ends with sulfobetaine zwitterions for perovskite coordination. Notably, these zwitterionic oligofluorenes are compatible with the hot injection and ligand exchange conditions used to prepare $CsPbBr_3$ NCs, yielding stable NC dispersions with high photoluminescence quantum yields (PLQY, >90%) and spectral features representative of both the perovskite core and conjugated ligand shell. Controlling the chain length of these capping ligands effectively regulated inter-NC spacing and packing geometry when cast into solid films, with evidence derived from both transmission electron microscopy (TEM) and grazing incidence X-ray scattering measurements.

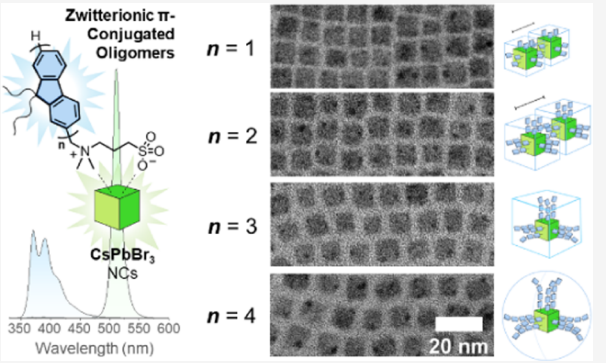

INTRODUCTION

Lead halide perovskite nanocrystals (NCs) are an emerging class[1] of bright, narrow line width nanoemitters that are especially unique for their soft, low-energy ionic lattice[2] and innate defect tolerance[3] that obviates the need for overcoating steps to achieve high photoluminescence quantum yields (PLQYs). Importantly, perovskite NC syntheses utilize abundant precursors (e.g., $PbBr_2$, CH_3NH_3Br, and Cs_2CO_3) that may be assembled via low-temperature ionic metathesis reactions[4,5] into a perovskite framework that, despite proliferation of A-site (e.g., Cs^+) and X-site (e.g., Br^-) vacancies,[6,7] has exceptionally robust emission. As detailed by Protesescu et al.,[8] the emission wavelength of all-inorganic $CsPbX_3$ NCs (where X = Cl, Br, I, or combinations thereof) is tunable across the visible spectrum (ca. 400−700 nm) by changing the halide composition, with quantum size effects playing a lesser role for the most common NC morphologies (i.e., nanocubes with 10 nm edge lengths). Subsequently, $CsPbX_3$ NCs were found to participate in rapid anion (halide) exchange reactions[9,10] with their surroundings, enabled by their mobile, vacancy-laden halide sublattice, thus opening routes to post-synthesis color tuning via simply mixing NCs with an external halide source (e.g., ammonium halides,[9−11] metal halide salts,[9,10] or others[12,13]). This host of useful properties have driven studies of perovskite NCs in lasing,[14] detection and imaging,[15] photocatalysis,[16] quantum emitters,[17] and LEDs,[18−20] where research continues at a rapid pace.

Semiconductor NCs as colloidal "inks" are amenable to solution-casting, which is advantageous over high-temperature, vacuum deposition methods often needed for their bulk counterparts; however, a classic trade-off to their use in solid-state devices is the presence of an insulating aliphatic ligand shell on their surface after synthesis. Ligands such as oleylamine and oleic acid are critical ingredients for NC synthesis—necessary to solubilize the Cs^+ and Pb^{2+} precursors and render the resulting $CsPbXr_3$ NCs colloidally stable; however, they may create a dielectric barrier that impedes charge carrier mobility through NC films, especially when present in excess. Significant efforts[21−23] have been dedicated to refining the NC purification conditions to purge the unbound ligand without compromising NC integrity. This is a delicate balance, as repetitive washing with polar solvents eventually removes the entire ligand shell (leading to sintering) and degrades the NC surface. The use of tight-binding ligands, such as *N,N*-dimethyl quaternary ammonium bromides[24] or zwitterions,[25] has helped to address these NC stability issues,

Received: November 13, 2023
Revised: February 18, 2024
Accepted: February 20, 2024
Published: March 12, 2024

https://doi.org/10.1021/jacs.3c12723
J. Am. Chem. Soc. 2024, 146, 8189−8197

Scheme 1. (Blue, (a)) Chain Building Steps Assembling the Oligofluorene Backbone via Iterative SM-Couplings and (Green, (b)) Conversion of the Chain-End Aldehydes of the n = 1−4 Oligomer Sulfobetaine Groups[a]

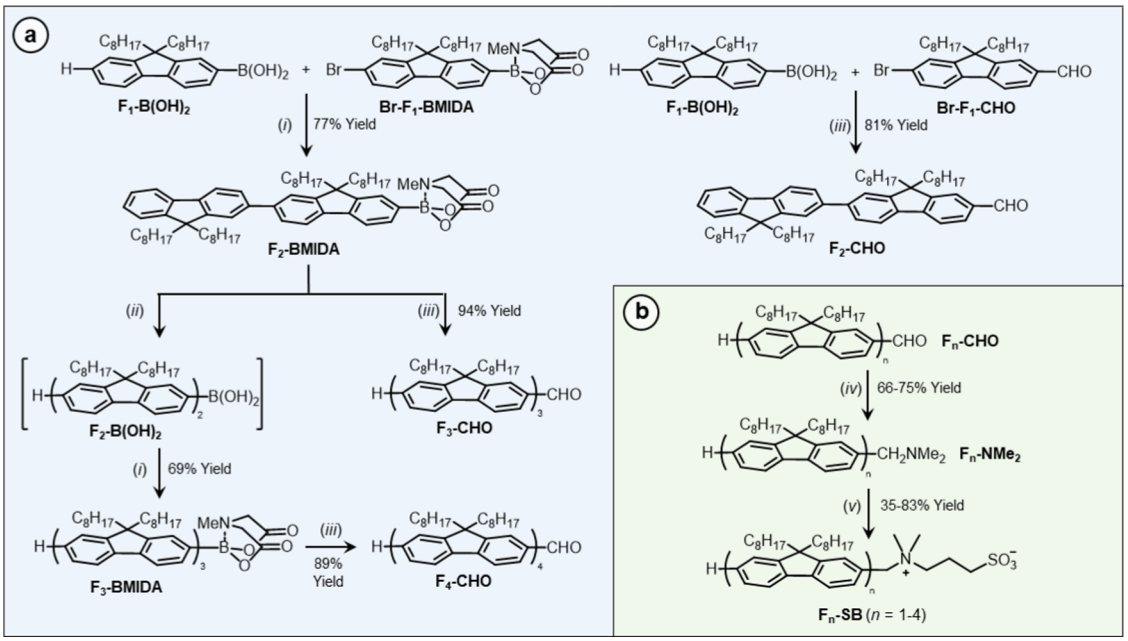

[a](i) $Pd(OAc)_2$/RuPhos/K_3PO_4/THF, 70 °C, 8 h; (ii) THF/NaOH(aq), RT; (iii) Br−F1−CHO/$Pd(PPh_3)4$/Aliquat 336/toluene/K_2CO_3(aq) 80 °C, 12 h; (iv) $HNMe_2$/$Ti(OiPr)_4$/THF/MeOH/$NaBH_4$, RT; and (v) 1,3-propanesultone/MeCN/acetone, 80 °C, 12−24 h.

permitting multiple precipitation steps to reduce ligand concentrations down to an approximately single-layer thick coating. Going further, several groups reported strategies to eliminate long-chain aliphatic ligands, including (a) resurfacing the NCs with an inorganic salt shell solely comprising Na^+ and Br^- ions, which dramatically enhanced charge carrier mobility in NC-based LEDs,[20] and (b) using aromatic ligands such as anilinium,[18] benzyl and phenalkylammonium,[26,27] and cinnamyl ammonium,[28] much in the same way that π-conjugated ligands were previously combined with metal chalcogenide QDs.[29−31] The latter approach has shown promise in devices in terms of lower turn-on voltages and improved efficiencies. However, the cited examples have a limited extent of π-conjugation and rely on weakly binding ammonium and anilinium cations to bring the aromatic ligands into close association with the perovskite surface. Other examples include our own group's work on benzyl ammonium-containing conjugated polymers used to grow $CsPbBr_3$ NCs[32] as well as a study by Liang et al., wherein $CsPbBr_3$ NCs were grown in a nanoreactor comprising poly(3-hexylthiophene) tethered to the chain ends of a poly(acrylic acid) star polymer.[33] While there are obvious motivations for merging the excellent optoelectronic properties of lead halide perovskites and π-conjugated polymers and oligomers, at present, there is a limited understanding of the interface between these material classes, which, in turn, is due to the limited synthetic tools available to access them.

Zwitterions exhibit tight coordination to lead halide perovskite surfaces—a feature attributed to simultaneous binding (i.e., chelation) of the zwitterion cation and anion head groups to adjacent pairs of A- and X-site vacancies.[25] By comparison, more conventional ligands such as primary ammonium halide salts exist in a state of dynamic exchange with $CsPbBr_3$ surfaces and can easily desorb following multiple NC precipitations into the polar solvent.[34] Conjugated polymer zwitterions (CPZs) are therefore a natural pairing with perovskite NCs, conferring strong stability and anchoring the conjugated backbone in the proximity of the perovskite surface. The CPZs previously reported by our group[35−38] and others[39,40] contain multiple zwitterions along the polymer chain, and as such, they dissolve as aqueous solutions or in polar organic solvents. This solubility is favorable for high-fidelity interlayers of organic photovoltaic (OPV) devices[41] but problematic for perovskite NCs, which require low-polarity solvents such as hexanes or toluene. Relocating the zwitterionic moiety to the polymer chain-end affords structures that combine the ligand coordination of zwitterions with apolar solvent compatibility. Along these lines, we report the first examples of conjugated oligomers/polymers (based on oligofluorene chains) with ω-chain-end sulfobetaine groups positioned in the proximity of the conjugated backbone. This new class of CPZs is readily integrated into existing procedures for $CsPbBr_3$ NC synthesis and ligand exchange, delivering perovskite NCs with an intimately attached, single layer of wide band gap semiconductor ligands.

RESULTS AND DISCUSSION

Sulfobetaine (SB)-terminated oligofluorene ligands (n = 1−4) were prepared in two stages: (1) a series of iterative Suzuki couplings (Scheme 1a) to generate the oligofluorene chain and (2) reductive amination and ring opening at the chain end to furnish the SB zwitterion (Scheme 1b). Key to this strategy was the use of *N*-methylimidodiacetic acid (MIDA) as the boronic acid protecting group in Suzuki−Miyaura (SM) cross-coupling. Under anhydrous SM conditions, free boronic acids reacted selectively in the presence of their MIDA-complexed counterparts, with the MIDA group removed later by stirring in an aqueous base. Using MIDA-protected haloboronic acids (e.g., **Br−F$_1$-BMIDA**, Scheme 1a), repeated coupling and deprotection result in step-by-step growth of complex

https://doi.org/10.1021/jacs.3c12723
J. Am. Chem. Soc. 2024, 146, 8189−8197

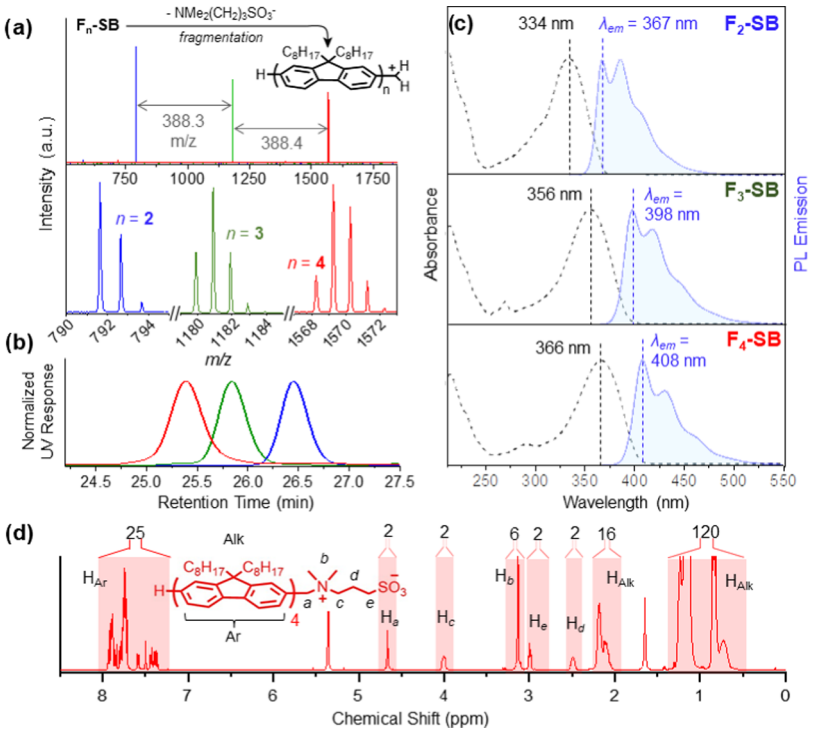

Figure 1. Characterization of zwitterionic oligofluorene ligands. (a) MALDI-TOF mass data show single peaks corresponding to a mass fragment originating from loss of $NMe_2(CH_2)_3SO_3^-$. (b) Narrow elution profiles observed by gel permeation chromatography (GPC) in THF confirm the uniform and increasing chain length for each oligomer ($F_2 \rightarrow F_4$). (c) Overlaid UV−vis and PL spectra. PL spectra were recorded with the excitation wavelengths set to the labeled absorption maximum of each oligomer. (d) ^1H NMR (500 MHz, CD_2Cl_2) of the F_4−SB ligand clearly showing a chain-end SB group.

polyaromatic scaffolds,[42−44] an example being the sequence-defined, regiospecific π-conjugated polymers recently reported by Xu et al.[45] The MIDA protection strategy was selected for this work owing to its relatively high throughput and ease of purification,[46] good control over chain length, and an ability to differentiate the chemistry of the α and ω chain ends, though we appreciate other, potentially useful methods such as those based on chromatography of oligomer mixtures.[47]

The oligomerization sequence began with the SM coupling of 9,9′-dioctylfluorene-2-boronic acid (**F_1-B(OH)$_2$**) with the MIDA-protected 2-bromo-9,9′-dioctylfluorene-7-boronic acid (**Br−F_1-BMIDA**). The latter was synthesized in two steps from 2,7-dibromo-9,9′-dioctylfluorene via borylation and MIDA protection, giving the monomer **Br−F_1-BMIDA** in good yield (71%) on a multigram scale. The **F_1-B(OH)$_2$** + **Br−F_1-BMIDA** SM cross-coupling gave the dimer **F_2-BMIDA** in a good yield (77%), which was either chain-capped with 2-bromo-9,9′-di-*n*-octylfluorene-7-carboxaldehyde (**Br−F_1-CHO**) to produce a trimer with chain-end aldehyde (**F_3-CHO**) or advanced into further iterations of chain growth. Using the fluorene-based chain-capping reagents **F_1-B(OH)$_2$** and **Br−F_1-CHO** (as opposed to simpler boronic acids such as *p*-tolylboronic acid[45]) reduced (by 2x) the number of deprotection and coupling iterations needed to reach the target oligomer, thus simplifying the process. Chain elongation of **F_2-BMIDA** proceeded by stirring the dimer as a solution in degassed THF with $NaOH_{(aq)}$, converting the MIDA group to the free boronic acid **F_2-B(OH)$_2$**, which was then coupled with **Br−F_1-BMIDA** to afford **F_3-BMIDA** (69% yield). Both **F_2-BMIDA** and **F_3-BMIDA** were capped with **Br−F_1-CHO** by reacting the MIDA-protected oligomers under aqueous SM coupling conditions, using $K_2CO_{3(aq)}$ to both remove the MIDA protecting groups in situ[48,49] and activate the resulting boronic acid. Chain capping in this manner afforded the tri- (**F_3-CHO**, 94% yield) and tetrameric (**F_4-CHO**, 89% yield) aldehydes; similar chemistry whereby the **F_1-B(OH)$_2$** and **Br−F_1-CHO** chain cappers were coupled directly furnished the dimer aldehyde (**F_2-CHO**, 81% yield). The unimer 9,9′-dioctylfluorene-2-carboxaldehyde (**F_1-CHO**) was synthesized via formylation of 9,9′-dioctyl-2-bromofluorene based on previously reported methods.[50] While the tetramer was the longest ligand we prepared, in principle, this iterative strategy may be repeated to reach longer chain lengths, noting that oligofluorenes reach full conjugation length at DP ∼ 10.[51]

Conversion of the chain-end aldehydes of the **F_1-CHO** through **F_4-CHO** series to SB groups was accomplished in two steps: (1) reductive amination with $HNMe_2/Ti(OiPr)_4$ followed by addition of $NaBH_4$,[52] affecting aldehyde to *N*,N-dimethylamine conversion (**F_n-NMe$_2$**), and (2) ring-opening of 1,3-propane sultone with the **F_n-NMe$_2$** oligomers. This yielded the corresponding **F_n-SB** zwitterions as solid powders that dissolved easily in toluene or $CHCl_3$—useful solvents for performing experiments with perovskite NCs. MALDI-TOF and GPC (Figure 1a,b) confirmed the discrete chain lengths of these zwitterionic oligofluorenes; in MALDI-TOF, an $[M - (CH_3)_2N(CH_2)_3SO_3]^+$ mass fragment (corresponding to a benzylic cation generated by loss of *N*,*N*-dimethylaminopropyl sulfonate) was observed for all **F_n-SB**. The SB resonances were visible by ^1H NMR spectroscopy in CD_2Cl_2 (4.67, 4.00, 3.00, 3.14, and 2.49 ppm), with integration against the aromatic protons (7.3−8.0 ppm) consistent with the expected chain length (Figure 1d). UV−vis and PL spectra of solutions of **F_2-SB** through **F_4-SB** in THF showed a shift in absorption (334−381 nm) and PL emission maxima (367−408 nm) to longer

https://doi.org/10.1021/jacs.3c12723
J. Am. Chem. Soc. 2024, 146, 8189−8197

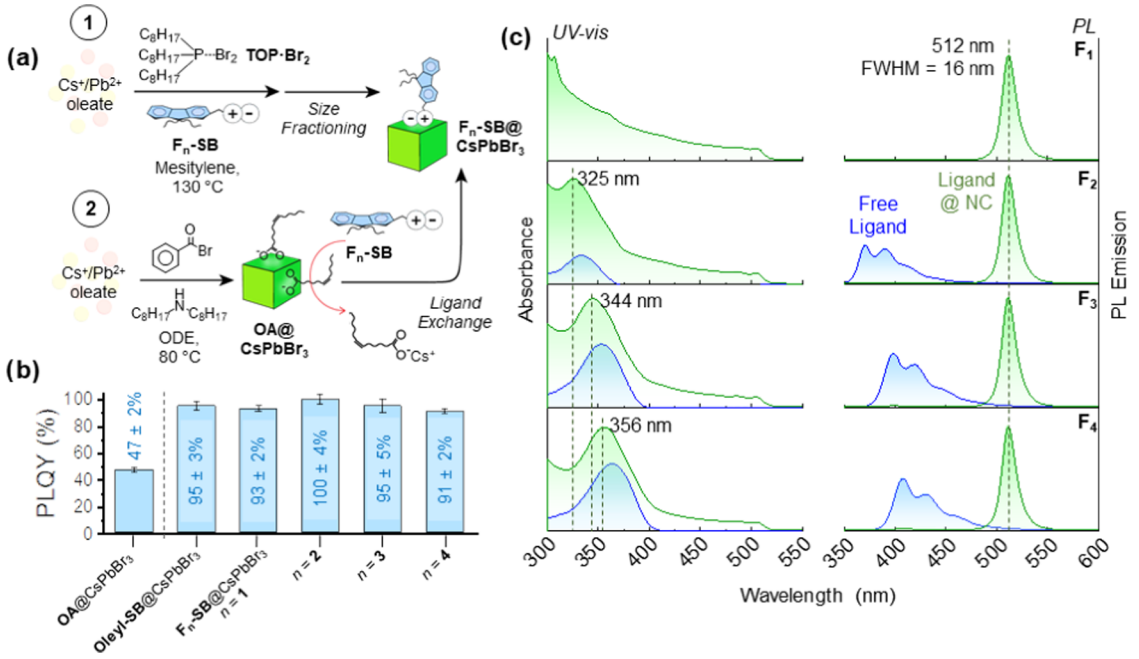

Figure 2. (a) Synthetic routes to oligofluorene-capped $CsPbBr_3$ NCs, involving either hot injection directly in the presence of $\mathbf{F_n}$**-SB** ligands (1) or synthesis of oleate-capped $CsPbBr_3$ NCs (**OA@CsPbBr$_3$**) followed by ligand exchange with $\mathbf{F_n}$**-SB** ligands. (b) Comparison of PLQY values for **OA@CsPbBr$_3$** NCs before and after ligand exchange, demonstrating the strong passivating effect of zwitterions. (c) Overlay of UV−vis and PL spectra for the $\mathbf{F_n}$**-SB@CsPbBr$_3$** NCs prepared via ligand exchange. PL spectra were recorded with excitation wavelengths set to the values of the labeled absorption maxima.

wavelengths with increasing n, resembling the known optical properties of nonfunctionalized oligofluorenes (Figure 1c).[51]

The $\mathbf{F_n}$**-SB** oligomers with their zwitterion "head" and conjugated "tail"—flanked by pairs of n-octyl chains on each repeat unit—resemble conventional zwitterionic surfactants,[25,53,54] and we found them useful in both the NC synthesis and ligand exchange. Adding $\mathbf{F_n}$**-SB** directly to the $CsPbBr_3$ NC growth procedure was enabled by the excellent solubility of the $\mathbf{F_n}$**-SB** oligomers in high-boiling solvents, such as mesitylene, used in the colloidal hot injection. In a typical procedure, the $\mathbf{F_n}$**-SB** ligand was dissolved in a mesitylene solution of cesium and lead oleate salts and heated to 130 °C, followed by injection of a tri-n-octylphosphine·Br_2 complex (TOP·Br_2) to form $CsPbBr_3$. The resulting $\mathbf{F_n}$**-SB@CsPbBr$_3$** NCs tend to have a wide range of initial shapes and sizes, typical of these zwitterion-based methods.[54] Size-selective precipitation was performed by washing the $\mathbf{F_n}$**-SB@CsPbBr$_3$** solution with acetone in small increments; for $\mathbf{F_1}$**-SB@CsPbBr$_3$** NCs, this resulted in multiple size fractions with edge lengths in the range of 6−8 nm, PL emission centered between 495 and 507 nm (fwhm = 20−21 nm), and a total combined $CsPbBr_3$ yield of 75% (Figures S1 and S2). Similar results were obtained using the $\mathbf{F_2}$**-SB** through $\mathbf{F_4}$**-SB** ligands, although longer ligands tended to produce smaller NCs that deviated from a cuboidal morphology, and accurate determination of PLQY was challenging in some cases (Figures S3−S8). Overall, this method produced high-quality, brightly fluorescent $CsPbBr_3$ NCs surface-functionalized with $\mathbf{F_n}$**-SB** oligomers.

We also studied ligand exchange using $\mathbf{F_n}$**-SB** ligands and $CsPbBr_3$ NCs. The NCs used in these experiments were prepared using the secondary amine method of Imran,[55] which gives an oleate-rich ligand shell. Replacing primary amines (e.g., oleylamine) in typical $CsPbX_3$ syntheses,[8,12] where their reversible surface binding as protonated ammonium salts is thought to promote anisotropic growth[55,56] and give mixtures of nanocubes and platelets, with secondary amines (e.g., dioctylamine, DOAm), which bind $CsPbX_3$ less effectively, improves NC shape and size homogeneity.[55] In addition, the oleate coating on these NCs is readily displaced by other ligands, for example, quaternary ammonium halides,[57] resulting in efficient exchange. In our hands, the synthesis of oleate-capped $CsPbBr_3$ NCs gave size uniform nanocubes (8.4 ± 0.5 nm) with narrow PL emission (fwhm = 17 nm) centered at 511 nm and moderate PLQY (47 ± 2%). Remarkably, adding small amounts of the $\mathbf{F_n}$**-SB** zwitterions (0.2−0.6 mg of $\mathbf{F_n}$**-SB**/mg of $CsPbBr_3$, corresponding to ca. 1.3 ligands·nm^{-2}) to these oleate-capped NCs, followed by stirring and precipitation into acetone, resulted in a dramatic PLQY boost (91−99%). A similar surface passivation and PL brightening were observed when adding oleyl sulfobetaine (oleyl-SB), demonstrating the impact of the zwitterion head group in perovskite surface stabilization. Control experiments, performed by omitting the zwitterion and precipitating the oleate-capped NCs directly into acetone, yielded a yellow, nonluminescent precipitate that failed to redisperse in toluene. Reanalyzing these $\mathbf{F_n}$**-SB@CsPbBr$_3$** and **oleyl-SB@CsPbBr$_3$** solutions after 6 months of storage under an inert atmosphere revealed excellent retention of PLQY for $\mathbf{F_2}$**-SB** through $\mathbf{F_4}$**-SB** (>90%) and only a slight decrease for NCs with $\mathbf{F_1}$**-SB** as a ligand (78%); on the other hand, $CsPbBr_3$ NCs capped with oleyl-SB largely sedimented during this period, preventing accurate determination of their solution absorbance/PL. The sterics of $\mathbf{F_2}$**-SB** through $\mathbf{F_4}$**-SB** may provide an additional layer of protection against NC sintering and degradation. After two ligand exchange steps, it is possible to reduce the residual oleic acid/oleate concentration to 0.1 mM, comprising ≤10% of the resulting ligand shell; notably, despite the different sizes of $\mathbf{F_1}$**-SB** through $\mathbf{F_4}$**-SB**,

https://doi.org/10.1021/jacs.3c12723
J. Am. Chem. Soc. 2024, 146, 8189−8197

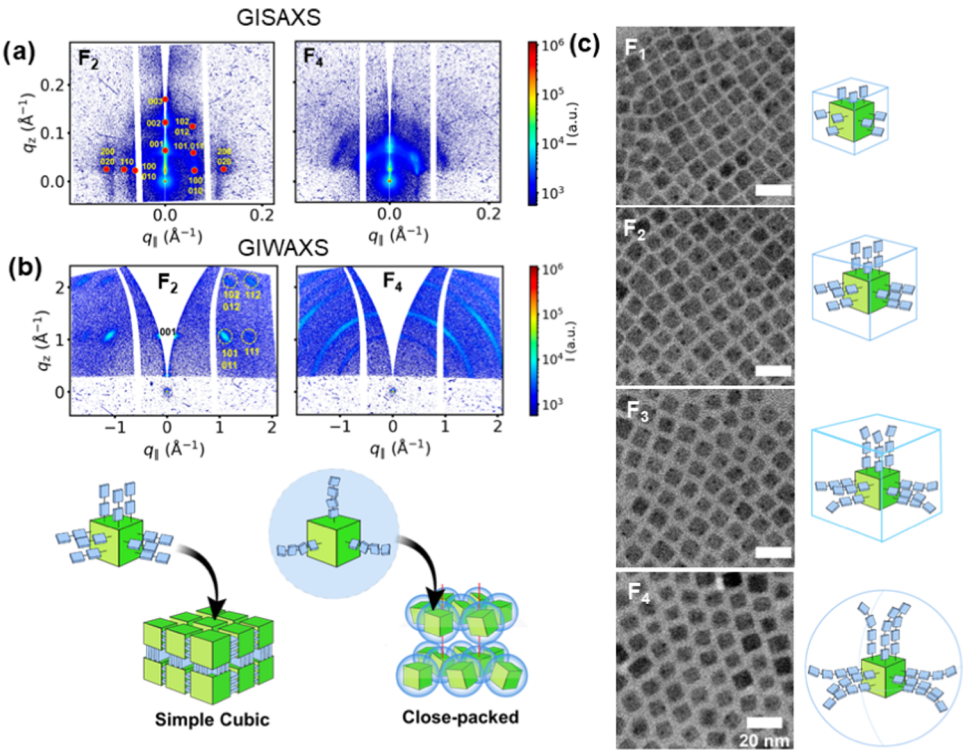

Figure 3. (a) GISAXS measurements of $\mathbf{F}_n$**-SB@CsPbBr$_3$** NCs n = 1−4 prepared via ligand exchange on OA@CsPbBr$_3$ NCs, cast as a film on the silicon substrate, which show a gradual shift in the distance between packing planes in the in-plane scattering direction as well as a transition from simple cubic to close-packed arrangement of the NCs in the film. (b) Azimuthal broadening for the **F$_4$-SB@CsPbBr$_3$** NC film suggests that the longer ligand disrupts any orientational preference of the NC with respect to the underlying substrate. (c) TEM images of these same NCs showing inter-NC distance to increase with ligand length.

their grafting density on the CsPbBr$_3$ surface is approximately the same (ρ = 1.0−1.3 ligands·nm^{-2}, determined by quantitative NMR spectroscopy performed on digested NC samples using 1,2,4,5-tetrachloro-3-nitrobenzene as an internal standard). Compared to $\mathbf{F}_n$**-SB@CsPbBr$_3$** NCs prepared by direct synthesis, the NCs produced by ligand exchange have a more consistent morphology and were easier to isolate and characterize, and all of the following examples of $\mathbf{F}_n$**-SB@CsPbBr$_3$** NCs in the text were prepared via this method.

Inspection of the UV−vis absorbance spectra in the $\mathbf{F}_n$**-SB@CsPbBr$_3$** NC series shows composite features of both the oligofluorene shell and the underlying CsPbBr$_3$ core (Figure 2). However, excitation of these $\mathbf{F}_n$**-SB@CsPbBr$_3$** NCs at the absorption maximum of the conjugated ligand (307−366 nm) produced PL spectra dominated by CsPbBr$_3$ emission, with only trace detectable oligofluorene PL. PL spectra of $\mathbf{F}_n$**-SB** (free ligand) and $\mathbf{F}_n$**-SB@CsPbBr$_3$** (NC-bound ligand) solutions (prepared at the same mg/mL ligand concentration, Figures 2 and S12) illustrate the order-of-magnitude extent of ligand PL suppression in the presence of the NCs, a characteristic of electronic communication between the conjugated ligand shell and perovskite NC core. In contrast, mixing **oleyl-SB@CsPbBr$_3$** NCs with the nonfunctionalized **F$_4$** tetramer (i.e., no zwitterion) in a control experiment led to no PL suppression of the ligand (Figure S13). Additional experiments measuring the PL excitation spectra of these samples over a series of dilutions were also insightful (Figure S21−S23). PL excitation spectra recorded at an emission wavelength of 512 nm (i.e., emission associated with the CsPbBr$_3$ NC, which does not overlap with the ligand PL) provide information about which component of the system (ligand or NC) absorbs incident light for NC re-emission. For **F$_4$-SB@CsPbBr$_3$**, at ≤5.5 nM NC, a prominent peak at 360 nm is seen in the PL excitation spectrum, suggesting absorption by the **F$_4$-SB** ligand, followed by an excited-state transfer from the ligand to the NC that results in NC emission. In contrast, no such peak was observed in the PL excitation spectra for **oleyl-SB@CsPbBr$_3$** with or without the added **F$_4$** tetramer (non-zwitterionic). Instead, only PL signatures of the CsPbBr$_3$ NC are seen, providing additional evidence for NC−ligand communication when the conjugated backbone is anchored to the NC. Moreover, to rule out PL quenching of the ligand by steric crowding at the NC surface (e.g., by excimer formation), we prepared systems with lower graft density of the **F$_4$-SB** ligand (ρ = 0.43 and 0.15 ligands·nm^{-2}) by ligand exchanging with mixtures of **F$_4$-SB** and **oleyl-SB** (Figure S24). In both cases, PL quenching was unaffected by the graft density, suggesting that quenching originates via NC−ligand interactions.

Casting $\mathbf{F}_n$**-SB@CsPbBr$_3$** NCs as solid films on quartz or silylated glass resulted in similar spectral features as in solution, although the CsPbBr$_3$ PL emission was red-shifted to 518−521 nm and slightly broadened (fwhm = 18−21 nm, Figure S13). A series of stability measurements on these films after annealing at 120 °C for 1 h or immersing in methanol for extended periods (Figure S25) showed a clear trend with respect to increasing ligand length and resilience to heat/polar solvent, whereas the solid-state PL of short chain-capped **oleyl-SB** or **F$_1$-SB@CsPbBr$_3$** NCs was cut in half after annealing at 120 °C—and nearly depleted after short periods in contact with methanol; these PL losses are significantly reduced NCs capped with the **F$_2$-SB** through **F$_4$-SB** ligands. Films prepared

https://doi.org/10.1021/jacs.3c12723
J. Am. Chem. Soc. 2024, 146, 8189−8197

from F_4-SB@CsPbBr$_3$ NCs were by far the most stable, retaining high percentages of their initial PL after thermal (79%) and polar solvent treatment (70%, submerged for 15 min in methanol); it is clear that progressively increasing the ligand chain length affords distinct advantages in terms of NC durability and processability, which may prove useful in their eventual application. In order to confirm the binding of oligofluorene zwitterions to the perovskite surface, ^{1}H NMR spectroscopy of the free F_4-SB ligand in C_6D_6 was compared with that of the F_4-SB@CsPbBr$_3$ NCs, with the latter showing disappearance of the zwitterion resonances and significant line broadening of the aromatic region, likely due to slow tumbling of the NCs in solution.[58] This line broadening was alleviated after digesting the F_4-SB@CsPbBr$_3$ NCs in DMSO-d_6, in keeping with previous studies on sulfobetaine ligands for CsPbBr$_3$ (Figure S14).[25] Additional evidence for attachment of the oligofluorene zwitterions to the CsPbBr$_3$ NC comes from DLS measurements, which show a trend in the z-average hydrodynamic diameter of the F_n-SB@CsPbBr$_3$ NCs at d_Z = 14.7−17.8 nm as the ligand length grows at n = 2−4 (Figure S14).

Examining the F_n-SB@CsPbBr$_3$ NCs by transmission electron microscopy (TEM) revealed the preservation of the cuboidal morphology after ligand exchange, although in the case of F_4-SB@CsPbBr$_3$, the edges of the cubes are less well-defined. Image analysis of F_1-SB@CsPbBr$_3$ through F_4-SB@CsPbBr$_3$ showed a similar size (edge length) of individual NCs across the entire series (d_{NC} = ca. 9 nm), consistent with the similar PL emission wavelength (512 nm) associated with the perovskite core for all F_n-SB@CsPbBr$_3$ samples (Figures 3 and S9 and S10). Closer inspection of the TEM images in Figure 3 shows that longer ligands produced systematically larger inter-NC spacing as well as different NC arrangements (cubic with shorter ligands vs. hexagonal with longer ligands) as they array in a single layer on the TEM grid. These observations suggest that longer ligands disrupt the alignment between adjacent NC facets and override the innate packing tendency of hard nanocubes. While TEM provides a useful picture of NC assembly (∼1000 nm^2, as in Figure 3c), grazing incidence small-angle X-ray scattering (GISAXS) measurements of concentrated F_n-SB@CsPbBr$_3$ NC solutions drop-cast onto polished Si (Figure 3) probe long-range order (3 mm^2 sampling area) and bulk morphology across the entire substrate (i.e., from center to edge). Both F_1-SB@CsPbBr$_3$ and F_2-SB@CsPbBr$_3$ formed films with simple cubic packing, with the latter exhibiting the most regular cubic structure. Indexing the GISAXS for F_2-SB@CsPbBr$_3$ NCs using a primitive cubic lattice is shown in Figure 3. A gradual transition in the packing geometry was observed for films of F_3-SB@CsPbBr$_3$, where the scattering pattern reflects the presence of mixed domains with cubic and close-packed (i.e., face-centered cubic or hexagonal close-packed) geometry. For NCs capped with F_4-SB@CsPbBr$_3$, the film exclusively shows a close-packed hexagonal structure, potentially due to the longer ligands projecting from the NC surface present a soft or "fuzzy" sphere instead of a hard cube. It is also possible that the loss of the nanocube edge definition (as noted above for F_4-SB@CsPbBr$_3$) contributes to changes in packing geometry. In-plane scattering was used to estimate the nearest neighbor distances for these samples, taking into account the differences in film morphology. For F_1-SB@CsPbBr$_3$ through F_3-SB@CsPbBr$_3$, a simple cubic packing was assumed and the nearest neighbor distance was estimated as $\delta = a_{sc} - d_{NC}$, whereas for F_4-SB@CsPbBr$_3$, hexagonal packing was assumed with a nearest neighbor distance of $\delta = ((3)^{1/2}/2)a_{hp} - d_{NC}$ (where a_{sc} and a_{hp} are the average distances between packing planes for cubic and hexagonal-packed structures, respectively—calculated as $2\pi/q^*$, with q^* being the primary scattering vector—and d_{NC} is the cube edge length estimated by TEM). We find that the values of δ trend from 1.0, 1.6, 3.3, and 4.1 nm for F_1-SB@CsPbBr$_3$ through F_4-SB@CsPbBr$_3$, consistent with the spacings observed by TEM. Given that the monomer length of a single fluorene repeat unit is estimated[59] to be 7.5 Å (and assuming that the ligands exist on the NC surface as fully extended rigid rods), the inter-NC spacings derived from TEM and X-ray scattering imply interdigitation of the conjugated ligands between adjacent NCs or that the chain axis of the oligofluorene backbone does not extend normal to the NC surface. Grazing incidence wide-angle X-ray diffraction (GIWAXD) measurements on this same series of samples show no azimuthal broadening of the diffractions for F_n-SB@CsPbBr$_3$ NC films when n = 1 or 2, suggesting that the (001) plane of the cubic CsPbBr$_3$ crystal lattice aligns parallel with the Si substrate (i.e., the cubic NCs align face on with the substrate). The indexing of reflections using a primitive cubic lattice is marked in Figure 3b. The ratio between the scattering vector of those diffractions turns out to be $1:\sqrt{2}:\sqrt{3}:2:\sqrt{5}:\sqrt{6}$, arising from crystal planes (001), (101) or (011), (111), (012) or (102), and (112), accordingly, confirming the face-on orientation of the NC on the substrate. The face-on orientation of NCs on the substrate allowed the third index, l of (hkl), to be identified unambiguously. The first two indices, h and k, are not distinguishable due to the NC freely rotating along the normal direction of the substrate. On the contrary, for F_n-SB@CsPbBr$_3$ NC films, where n = 3 or 4, there is significant azimuthal broadening, as longer ligands disrupt any orientational preference of the NCs with respect to the underlying substrate. While the results for F_1-SB and F_2-SB@CsPbBr$_3$ NCs were consistent with previous studies showing packing of aliphatic ligand-capped perovskite nanocubes into well-ordered cubic superlattices,[60,61] clearly, the longer ligands disrupt face-on inter-NC and NC-substrate alignment in these films.

Notably, casting F_2-SB@CsPbBr$_3$ NC films under slightly different conditions (higher dilution on silylated glass) produced brightly fluorescent, micron-sized rectangles, formed at the edge of the drying NC solution, that were observable by confocal microscopy (Figures 4 and S18). These resemble the types of structures previously reported for perovskite NC superlattices, which have drawn interest due to their properties of collective emission (i.e., coherent coupling between quantum emitters in a long range-ordered, closely packed lattice that causes them to collectively behave as a large, single emitting dipole that releases a burst of superfluorescent radiation).[61,62] AFM imaging of an isolated F_2-SB@CsPbBr$_3$ superstructure in Figure 4 shows its lateral dimensions (16 μm × 19 μm) to be significantly greater than its height (0.5 μm). Similar types of structures were observed by confocal microscopy for NCs with F_3-SB and F_4-SB ligands (Figures S19 and S20). Since GIWAXS/GISAXS measurements sample a large area of the film, one cannot draw conclusions about NC packing within the superstructures based on the scattering data in Figure 3. While there are numerous examples of CsPbBr$_3$ NC superlattice formation using conventional aliphatic ligands,[54,55,61] given the relative size and complexity of F_n-SB ligands, the formation of such superstructures is remarkable

https://doi.org/10.1021/jacs.3c12723
J. Am. Chem. Soc. 2024, 146, 8189−8197

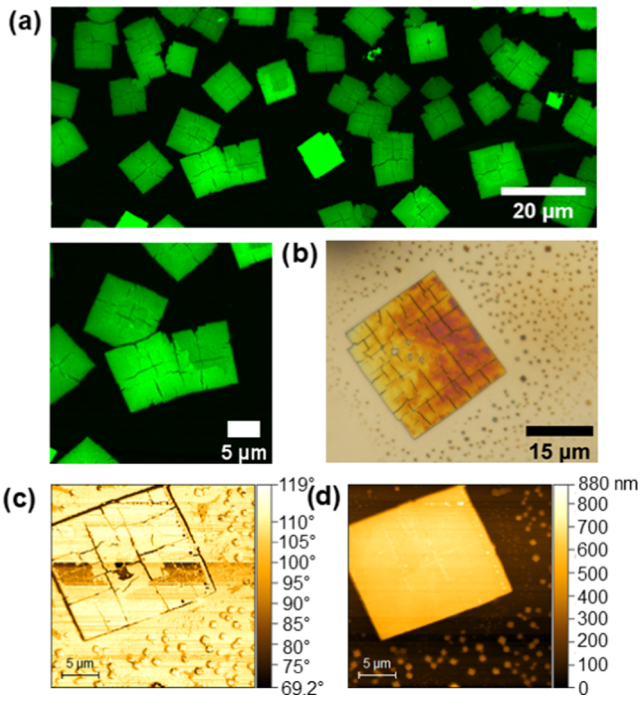

Figure 4. (a) Confocal fluorescence microscopy images of superstructures formed from F_2-SB@$CsPbBr_3$ NCs. Polarized optical light microscopy image (b) of one of these isolated superstructures on Si wafer. AFM phase (c) and height retrace (d) giving approximate dimensions of 16 μm × 19 μm × 0.5 μm for the assembled structure.

and brings the inherent utility of conjugated organics to ordered NC arrays.

CONCLUSIONS

A new series of zwitterion-capped π-conjugated ligands were prepared in good yields via an iterative synthesis strategy, giving well-defined oligomeric structures that were integrated effectively into perovskite NC syntheses. Compared with prior reports of conjugated polymer/oligomer zwitterions, repositioning the zwitterion to the chain end renders these oligomers soluble in the solution media needed to grow and handle $CsPbBr_3$ NCs (i.e., nonpolar hydrocarbons). Interactions between the sulfobetaine chain end and perovskite surface lead to close NC−ligand association, in which ligand binding fundamentally alters the nature of electronic communication between the NC core and oligomer shell. The iterative oligofluorene synthesis yields ligand structures that in turn control the inter-NC spacing and packing geometry in thin films while systematically dialing in optical properties of the hybrid structures. Despite the unique structure and size of these conjugated ligands, the resultant NCs remain amenable to the formation of large-area superstructures. We anticipate that this conjugated oligomer approach will be adaptable to other types of ligand chemistry, and envision this work to outline a general strategy for merging perovskite and organic semiconductors into hybrid structures with tunable electronic properties tailored for light-emitting, light-harvesting, and photocatalytic applications.

ASSOCIATED CONTENT

Supporting Information

The Supporting Information is available free of charge at https://pubs.acs.org/doi/10.1021/jacs.3c12723.

All ligand and nanocrystal syntheses, ligand exchange procedures, and substrate/sample preparation for characterization (DOCX)

AUTHOR INFORMATION

Corresponding Author

Todd Emrick − *Department of Polymer Science & Engineering, University of Massachusetts, Conte Center for Polymer Research, Amherst, Massachusetts 01003, United States;* orcid.org/0000-0003-0460-1797; Email: tsemrick@mail.pse.umass.edu

Authors

Christopher Cueto − *Department of Polymer Science & Engineering, University of Massachusetts, Conte Center for Polymer Research, Amherst, Massachusetts 01003, United States*

Mingqiu Hu − *Department of Polymer Science & Engineering, University of Massachusetts, Conte Center for Polymer Research, Amherst, Massachusetts 01003, United States*

Thomas P. Russell − *Department of Polymer Science & Engineering, University of Massachusetts, Conte Center for Polymer Research, Amherst, Massachusetts 01003, United States;* orcid.org/0000-0001-6384-5826

Complete contact information is available at: https://pubs.acs.org/10.1021/jacs.3c12723

Author Contributions

The article was written through contributions of all authors.

Funding

National Science Foundation (NSF-CHE-2203578), Mitsubishi Chemical

Notes

The authors declare no competing financial interest.

ACKNOWLEDGMENTS

The authors appreciate support for this work from the National Science Foundation (NSF-CHE-2203578) as well as Mitsubishi Chemical.

REFERENCES

(1) Dey, A.; Ye, J.; De, A.; Debroye, E.; Ha, S. K.; Bladt, E.; Kshirsagar, A. S.; Wang, Z.; Yin, J.; Wang, Y.; Quan, L. N.; Yan, F.; Gao, M.; Li, X.; Shamsi, J.; Debnath, T.; Cao, M.; Scheel, M. A.; Kumar, S.; Steele, J. A.; Gerhard, M.; Chouhan, L.; Xu, K.; Wu, X.; Li, Y.; Zhang, Y.; Dutta, A.; Han, C.; Vincon, I.; Rogach, A. L.; Nag, A.; Samanta, A.; Korgel, B. A.; Shih, C.-J.; Gamelin, D. R.; Son, D. H.; Zeng, H.; Zhong, H.; Sun, H.; Demir, H. V.; Scheblykin, I. G.; Mora-Seró, I.; Stolarczyk, J. K.; Zhang, J. Z.; Feldmann, J.; Hofkens, J.; Luther, J. M.; Pérez-Prieto, J.; Li, L.; Manna, L.; Bodnarchuk, M. I.; Kovalenko, M. V.; Roeffaers, M. B. J.; Pradhan, N.; Mohammed, O. F.; Bakr, O. M.; Yang, P.; Müller-Buschbaum, P.; Kamat, P. V.; Bao, Q.; Zhang, Q.; Krahne, R.; Galian, R. E.; Stranks, S. D.; Bals, S.; Biju, V.; Tisdale, W. A.; Yan, Y.; Hoye, R. L. Z.; Polavarapu, L. State of the Art and Prospects for Halide Perovskite Nanocrystals. *ACS Nano* **2021**, *15* (7), 10775−10981.

(2) Glasser, L. Lattice Energies of Crystals with Multiple Ions: A Generalized Kapustinskii Equation. *Inorg. Chem.* **1995**, *34* (20), 4935−4936.

(3) Kang, J.; Wang, L.-W. High Defect Tolerance in Lead Halide Perovskite $CsPbBr_3$. *J. Phys. Chem. Lett.* **2017**, *8* (2), 489−493.

(4) Zhang, F.; Zhong, H.; Chen, C.; Wu, X.; Hu, X.; Huang, H.; Han, J.; Zou, B.; Dong, Y. Brightly Luminescent and Color-Tunable Colloidal $CH_3NH_3PbX_3$ (X = Br, I, Cl) Quantum Dots: Potential

Alternatives for Display Technology. *ACS Nano* **2015**, *9* (4), 4533−4542.
(5) Li, X.; Wu, Y.; Zhang, S.; Cai, B.; Gu, Y.; Song, J.; Zeng, H. CsPbX3 Quantum Dots for Lighting and Displays: Room-Temperature Synthesis, Photoluminescence Superiorities, Underlying Origins and White Light-Emitting Diodes. *Adv. Funct. Mater.* **2016**, *26* (15), 2435−2445.
(6) Walsh, A.; Scanlon, D. O.; Chen, S.; Gong, X. G.; Wei, S.-H. Self-Regulation Mechanism for Charged Point Defects in Hybrid Halide Perovskites. *Angew. Chem., Int. Ed.* **2015**, *54* (6), 1791−1794.
(7) Kovalenko, M. V.; Protesescu, L.; Bodnarchuk, M. I. Properties and Potential Optoelectronic Applications of Lead Halide Perovskite Nanocrystals. *Science* **2017**, *358* (6364), 745−750.
(8) Protesescu, L.; Yakunin, S.; Bodnarchuk, M. I.; Krieg, F.; Caputo, R.; Hendon, C. H.; Yang, R. X.; Walsh, A.; Kovalenko, M. V. Nanocrystals of Cesium Lead Halide Perovskites ($CsPbX_3$, X = Cl, Br, and I): Novel Optoelectronic Materials Showing Bright Emission with Wide Color Gamut. *Nano Lett.* **2015**, *15* (6), 3692−3696.
(9) Nedelcu, G.; Protesescu, L.; Yakunin, S.; Bodnarchuk, M. I.; Grotevent, M. J.; Kovalenko, M. V. Fast Anion-Exchange in Highly Luminescent Nanocrystals of Cesium Lead Halide Perovskites ($CsPbX_3$, X = Cl, Br, I). *Nano Lett.* **2015**, *15* (8), 5635−5640.
(10) Akkerman, Q. A.; D'Innocenzo, V.; Accornero, S.; Scarpellini, A.; Petrozza, A.; Prato, M.; Manna, L. Tuning the Optical Properties of Cesium Lead Halide Perovskite Nanocrystals by Anion Exchange Reactions. *J. Am. Chem. Soc.* **2015**, *137* (32), 10276−10281.
(11) Cueto, C.; Hu, W.; Ribbe, A.; Bolduc, K.; Emrick, T. Polystyrene-Based Macromolecular Ammonium Halides for Tuning Color and Exchange Kinetics of Perovskite Nanocrystals. *Angew. Chem., Int. Ed.* **2022**, *61* (37), No. e202207126.
(12) Imran, M.; Caligiuri, V.; Wang, M.; Goldoni, L.; Prato, M.; Krahne, R.; De Trizio, L.; Manna, L. Benzoyl Halides as Alternative Precursors for the Colloidal Synthesis of Lead-Based Halide Perovskite Nanocrystals. *J. Am. Chem. Soc.* **2018**, *140* (7), 2656−2664.
(13) Creutz, S. E.; Crites, E. N.; De Siena, M. C.; Gamelin, D. R. Anion Exchange in Cesium Lead Halide Perovskite Nanocrystals and Thin Films Using Trimethylsilyl Halide Reagents. *Chem. Mater.* **2018**, *30* (15), 4887−4891.
(14) Zhu, H.; Fu, Y.; Meng, F.; Wu, X.; Gong, Z.; Ding, Q.; Gustafsson, M. V.; Trinh, M. T.; Jin, S.; Zhu, X.-Y. Lead Halide Perovskite Nanowire Lasers with Low Lasing Thresholds and High Quality Factors. *Nat. Mater.* **2015**, *14* (6), 636−642.
(15) Wei, H.; Fang, Y.; Mulligan, P.; Chuirazzi, W.; Fang, H.-H.; Wang, C.; Ecker, B. R.; Gao, Y.; Loi, M. A.; Cao, L.; Huang, J. Sensitive X-Ray Detectors Made of Methylammonium Lead Tribromide Perovskite Single Crystals. *Nat. Photon* **2016**, *10* (5), 333−339.
(16) Huynh, K. A.; Nguyen, D. L. T.; Nguyen, V.-H.; Vo, D.-V. N.; Trinh, Q. T.; Nguyen, T. P.; Kim, S. Y.; Le, Q. V. Halide Perovskite Photocatalysis: Progress and Perspectives. *J. Chem. Technol. Biotechnol.* **2020**, *95* (10), 2579−2596.
(17) Utzat, H.; Sun, W.; Kaplan, A. E. K.; Krieg, F.; Ginterseder, M.; Spokoyny, B.; Klein, N. D.; Shulenberger, K. E.; Perkinson, C. F.; Kovalenko, M. V.; Bawendi, M. G. Coherent Single-Photon Emission from Colloidal Lead Halide Perovskite Quantum Dots. *Science* **2019**, *363* (6431), 1068−1072.
(18) Chiba, T.; Hayashi, Y.; Ebe, H.; Hoshi, K.; Sato, J.; Sato, S.; Pu, Y.-J.; Ohisa, S.; Kido, J. Anion-Exchange Red Perovskite Quantum Dots with Ammonium Iodine Salts for Highly Efficient Light-Emitting Devices. *Nat. Photon* **2018**, *12* (11), 681−687.
(19) Chen, H.; Fan, L.; Zhang, R.; Bao, C.; Zhao, H.; Xiang, W.; Liu, W.; Niu, G.; Guo, R.; Zhang, L.; Wang, L. High-Efficiency Formamidinium Lead Bromide Perovskite Nanocrystal-Based Light-Emitting Diodes Fabricated via a Surface Defect Self-Passivation Strategy. *Adv. Opt. Mater.* **2020**, *8* (6), No. 1901390.
(20) Dong, Y.; Wang, Y.-K.; Yuan, F.; Johnston, A.; Liu, Y.; Ma, D.; Choi, M.-J.; Chen, B.; Chekini, M.; Baek, S.-W.; Sagar, L. K.; Fan, J.; Hou, Y.; Wu, M.; Lee, S.; Sun, B.; Hoogland, S.; Quintero-Bermudez, R.; Ebe, H.; Todorovic, P.; Dinic, F.; Li, P.; Kung, H. T.; Saidaminov, M. I.; Kumacheva, E.; Spiecker, E.; Liao, L.-S.; Voznyy, O.; Lu, Z.-H.; Sargent, E. H. Bipolar-Shell Resurfacing for Blue LEDs Based on Strongly Confined Perovskite Quantum Dots. *Nat. Nanotechnol.* **2020**, *15* (8), 668−674.
(21) Li, J.; Xu, L.; Wang, T.; Song, J.; Chen, J.; Xue, J.; Dong, Y.; Cai, B.; Shan, Q.; Han, B.; Zeng, H. 50-Fold EQE Improvement up to 6.27% of Solution-Processed All-Inorganic Perovskite $CsPbBr_3$ QLEDs via Surface Ligand Density Control. *Adv. Mater.* **2017**, *29* (5), No. 1603885.
(22) Chiba, T.; Hoshi, K.; Pu, Y.-J.; Takeda, Y.; Hayashi, Y.; Ohisa, S.; Kawata, S.; Kido, J. High-Efficiency Perovskite Quantum-Dot Light-Emitting Devices by Effective Washing Process and Interfacial Energy Level Alignment. *ACS Appl. Mater. Interfaces* **2017**, *9* (21), 18054−18060.
(23) Hoshi, K.; Chiba, T.; Sato, J.; Hayashi, Y.; Takahashi, Y.; Ebe, H.; Ohisa, S.; Kido, J. Purification of Perovskite Quantum Dots Using Low-Dielectric-Constant Washing Solvent "Diglyme" for Highly Efficient Light-Emitting Devices. *ACS Appl. Mater. Interfaces* **2018**, *10* (29), 24607−24612.
(24) Pan, J.; Quan, L. N.; Zhao, Y.; Peng, W.; Murali, B.; Sarmah, S. P.; Yuan, M.; Sinatra, L.; Alyami, N. M.; Liu, J.; Yassitepe, E.; Yang, Z.; Voznyy, O.; Comin, R.; Hedhili, M. N.; Mohammed, O. F.; Lu, Z. H.; Kim, D. H.; Sargent, E. H.; Bakr, O. M. Highly Efficient Perovskite-Quantum-Dot Light-Emitting Diodes by Surface Engineering. *Adv. Mater.* **2016**, *28* (39), 8718−8725.
(25) Krieg, F.; Ochsenbein, S. T.; Yakunin, S.; ten Brinck, S.; Aellen, P.; Süess, A.; Clerc, B.; Guggisberg, D.; Nazarenko, O.; Shynkarenko, Y.; Kumar, S.; Shih, C.-J.; Infante, I.; Kovalenko, M. V. Colloidal $CsPbX_3$ (X = Cl, Br, I) Nanocrystals 2.0: Zwitterionic Capping Ligands for Improved Durability and Stability. *ACS Energy Lett.* **2018**, *3* (3), 641−646.
(26) Vickers, E. T.; Graham, T. A.; Chowdhury, A. H.; Bahrami, B.; Dreskin, B. W.; Lindley, S.; Naghadeh, S. B.; Qiao, Q.; Zhang, J. Z. Improving Charge Carrier Delocalization in Perovskite Quantum Dots by Surface Passivation with Conductive Aromatic Ligands. *ACS Energy Lett.* **2018**, *3* (12), 2931−2939.
(27) Li, G.; Huang, J.; Li, Y.; Tang, J.; Jiang, Y. Highly Bright and Low Turn-on Voltage $CsPbBr_3$ Quantum Dot LEDs via Conjugation Molecular Ligand Exchange. *Nano Res.* **2019**, *12* (1), 109−114.
(28) Dai, J.; Xi, J.; Li, L.; Zhao, J.; Shi, Y.; Zhang, W.; Ran, C.; Jiao, B.; Hou, X.; Duan, X.; Wu, Z. Charge Transport between Coupling Colloidal Perovskite Quantum Dots Assisted by Functional Conjugated Ligands. *Angew. Chem., Int. Ed.* **2018**, *57* (20), 5754−5758.
(29) Milliron, Dj.; Alivisatos, Ap.; Pitois, C.; Edder, C.; Fréchet, J. m. j. Electroactive Surfactant Designed to Mediate Electron Transfer Between CdSe Nanocrystals and Organic Semiconductors. *Adv. Mater.* **2003**, *15* (1), 58−61.
(30) Liu, J.; Tanaka, T.; Sivula, K.; Alivisatos, A. P.; Fréchet, J. M. J. Employing End-Functional Polythiophene To Control the Morphology of Nanocrystal−Polymer Composites in Hybrid Solar Cells. *J. Am. Chem. Soc.* **2004**, *126* (21), 6550−6551.
(31) Skaff, H.; Sill, K.; Emrick, T. Quantum Dots Tailored with Poly(Para-Phenylene Vinylene). *J. Am. Chem. Soc.* **2004**, *126* (36), 11322−11325.
(32) Kim, H.; So, S.; Ribbe, A.; Liu, Y.; Hu, W.; Duzhko, V. V.; Hayward, R. C.; Emrick, T. Functional Polymers for Growth and Stabilization of $CsPbBr_3$ Perovskite Nanoparticles. *Chem. Commun.* **2019**, *55* (12), 1833−1836.
(33) Liang, S.; He, S.; Zhang, M.; Yan, Y.; Jin, T.; Lian, T.; Lin, Z. Tailoring Charge Separation at Meticulously Engineered Conjugated Polymer/Perovskite Quantum Dot Interface for Photocatalyzing Atom Transfer Radical Polymerization. *J. Am. Chem. Soc.* **2022**, *144* (28), 12901−12914.
(34) De Roo, J.; Ibáñez, M.; Geiregat, P.; Nedelcu, G.; Walravens, W.; Maes, J.; Martins, J. C.; Van Driessche, I.; Kovalenko, M. V.; Hens, Z. Highly Dynamic Ligand Binding and Light Absorption

Coefficient of Cesium Lead Bromide Perovskite Nanocrystals. *ACS Nano* **2016**, *10* (2), 2071−2081.
(35) Liu, F.; Page, Z. A.; Duzhko, V. V.; Russell, T. P.; Emrick, T. Conjugated Polymeric Zwitterions as Efficient Interlayers in Organic Solar Cells. *Adv. Mater.* **2013**, *25* (47), 6868−6873.
(36) Liu, Y.; Page, Z. A.; Russell, T. P.; Emrick, T. Finely Tuned Polymer Interlayers Enhance Solar Cell Efficiency. *Angew. Chem., Int. Ed.* **2015**, *54* (39), 11485−11489.
(37) Page, Z. A.; Liu, F.; Russell, T. P.; Emrick, T. Tuning the Energy Gap of Conjugated Polymer Zwitterions for Efficient Interlayers and Solar Cells. *J. Polym. Sci., Part A: Polym. Chem.* **2015**, *53* (2), 327−336.
(38) Page, Z. A.; Liu, Y.; Puodziukynaite, E.; Russell, T. P.; Emrick, T. Hydrophilic Conjugated Polymers Prepared by Aqueous Horner−Wadsworth−Emmons Coupling. *Macromolecules* **2016**, *49* (7), 2526−2532.
(39) Duan, C.; Wang, L.; Zhang, K.; Guan, X.; Huang, F. Conjugated Zwitterionic Polyelectrolytes and Their Neutral Precursor as Electron Injection Layer for High-Performance Polymer Light-Emitting Diodes. *Adv. Mater.* **2011**, *23* (14), 1665−1669.
(40) Fang, J.; Wallikewitz, B. H.; Gao, F.; Tu, G.; Müller, C.; Pace, G.; Friend, R. H.; Huck, W. T. S. Conjugated Zwitterionic Polyelectrolyte as the Charge Injection Layer for High-Performance Polymer Light-Emitting Diodes. *J. Am. Chem. Soc.* **2011**, *133* (4), 683−685.
(41) Liu, Y.; Duzhko, V. V.; Page, Z. A.; Emrick, T.; Russell, T. P. Conjugated Polymer Zwitterions: Efficient Interlayer Materials in Organic Electronics. *Acc. Chem. Res.* **2016**, *49* (11), 2478−2488.
(42) Gillis, E. P.; Burke, M. D. A Simple and Modular Strategy for Small Molecule Synthesis: Iterative Suzuki−Miyaura Coupling of B-Protected Haloboronic Acid Building Blocks. *J. Am. Chem. Soc.* **2007**, *129* (21), 6716−6717.
(43) Li, J.; Grillo, A. S.; Burke, M. D. From Synthesis to Function via Iterative Assembly of N-Methyliminodiacetic Acid Boronate Building Blocks. *Acc. Chem. Res.* **2015**, *48* (8), 2297−2307.
(44) Lehmann, J. W.; Blair, D. J.; Burke, M. D. Towards the Generalized Iterative Synthesis of Small Molecules. *Nat. Rev. Chem.* **2018**, *2* (2), 1−20.
(45) Xu, C.; He, C.; Li, N.; Yang, S.; Du, Y.; Matyjaszewski, K.; Pan, X. Regio- and Sequence-Controlled Conjugated Topological Oligomers and Polymers via Boronate-Tag Assisted Solution-Phase Strategy. *Nat. Commun.* **2021**, *12* (1), No. 5853, DOI: 10.1038/s41467-021-26186-y.
(46) Li, J.; Ballmer, S. G.; Gillis, E. P.; Fujii, S.; Schmidt, M. J.; Palazzolo, A. M. E.; Lehmann, J. W.; Morehouse, G. F.; Burke, M. D. Synthesis of Many Different Types of Organic Small Molecules Using One Automated Process. *Science* **2015**, *347* (6227), 1221−1226.
(47) Lawrence, J.; Goto, E.; Ren, J. M.; McDearmon, B.; Kim, D. S.; Ochiai, Y.; Clark, P. G.; Laitar, D.; Higashihara, T.; Hawker, C. J. A Versatile and Efficient Strategy to Discrete Conjugated Oligomers. *J. Am. Chem. Soc.* **2017**, *139* (39), 13735−13739.
(48) Knapp, D. M.; Gillis, E. P.; Burke, M. D. A General Solution for Unstable Boronic Acids: Slow-Release Cross-Coupling from Air-Stable MIDA Boronates. *J. Am. Chem. Soc.* **2009**, *131* (20), 6961−6963.
(49) Gonzalez, J. A.; Ogba, O. M.; Morehouse, G. F.; Rosson, N.; Houk, K. N.; Leach, A. G.; Cheong, P. H.-Y.; Burke, M. D.; Lloyd-Jones, G. C. MIDA Boronates Are Hydrolysed Fast and Slow by Two Different Mechanisms. *Nat. Chem.* **2016**, *8* (11), 1067−1075.
(50) Li, B.; Li, J.; Fu, Y.; Bo, Z. Porphyrins with Four Monodisperse Oligofluorene Arms as Efficient Red Light-Emitting Materials. *J. Am. Chem. Soc.* **2004**, *126* (11), 3430−3431.
(51) Klaerner, G.; Miller, R. D. Polyfluorene Derivatives: Effective Conjugation Lengths from Well-Defined Oligomers. *Macromolecules* **1998**, *31* (6), 2007−2009.
(52) Bhattacharyya, S. A High Throughput Synthesis of N,N-Dimethyl Tertiary Amines. *Synth. Commun.* **2000**, *30* (11), 2001−2008.
(53) Krieg, F.; Ong, Q. K.; Burian, M.; Rainò, G.; Naumenko, D.; Amenitsch, H.; Süess, A.; Grotevent, M. J.; Krumeich, F.; Bodnarchuk, M. I.; Shorubalko, I.; Stellacci, F.; Kovalenko, M. V. Stable Ultraconcentrated and Ultradilute Colloids of $CsPbX_3$ (X = Cl, Br) Nanocrystals Using Natural Lecithin as a Capping Ligand. *J. Am. Chem. Soc.* **2019**, *141* (50), 19839−19849.
(54) Krieg, F.; Sercel, P. C.; Burian, M.; Andrusiv, H.; Bodnarchuk, M. I.; Stöferle, T.; Mahrt, R. F.; Naumenko, D.; Amenitsch, H.; Rainò, G.; Kovalenko, M. V. Monodisperse Long-Chain Sulfobetaine-Capped $CsPbBr_3$ Nanocrystals and Their Superfluorescent Assemblies. *ACS Cent. Sci.* **2021**, *7* (1), 135−144.
(55) Imran, M.; Ijaz, P.; Baranov, D.; Goldoni, L.; Petralanda, U.; Akkerman, Q.; Abdelhady, A. L.; Prato, M.; Bianchini, P.; Infante, I.; Manna, L. Shape-Pure, Nearly Monodispersed $CsPbBr_3$ Nanocubes Prepared Using Secondary Aliphatic Amines. *Nano Lett.* **2018**, *18* (12), 7822−7831.
(56) Almeida, G.; Goldoni, L.; Akkerman, Q.; Dang, Z.; Khan, A. H.; Marras, S.; Moreels, I.; Manna, L. Role of Acid−Base Equilibria in the Size, Shape, and Phase Control of Cesium Lead Bromide Nanocrystals. *ACS Nano* **2018**, *12* (2), 1704−1711.
(57) Imran, M.; Ijaz, P.; Goldoni, L.; Maggioni, D.; Petralanda, U.; Prato, M.; Almeida, G.; Infante, I.; Manna, L. Simultaneous Cationic and Anionic Ligand Exchange For Colloidally Stable $CsPbBr_3$ Nanocrystals. *ACS Energy Lett.* **2019**, *4* (4), 819−824.
(58) Hens, Z.; Martins, J. C. A Solution NMR Toolbox for Characterizing the Surface Chemistry of Colloidal Nanocrystals. *Chem. Mater.* **2013**, *25* (8), 1211−1221.
(59) Fytas, G.; Nothofer, H. G.; Scherf, U.; Vlassopoulos, D.; Meier, G. Structure and Dynamics of Nondilute Polyfluorene Solutions. *Macromolecules* **2002**, *35* (2), 481−488.
(60) Nagaoka, Y.; Hills-Kimball, K.; Tan, R.; Li, R.; Wang, Z.; Chen, O. Nanocube Superlattices of Cesium Lead Bromide Perovskites and Pressure-Induced Phase Transformations at Atomic and Mesoscale Levels. *Adv. Mater.* **2017**, *29* (18), No. 1606666.
(61) Rainò, G.; Becker, M. A.; Bodnarchuk, M. I.; Mahrt, R. F.; Kovalenko, M. V.; Stöferle, T. Superfluorescence from Lead Halide Perovskite Quantum Dot Superlattices. *Nature* **2018**, *563* (7733), 671−675.
(62) Baranov, D.; Fieramosca, A.; Yang, R. X.; Polimeno, L.; Lerario, G.; Toso, S.; Giansante, C.; Giorgi, M. D.; Tan, L. Z.; Sanvitto, D.; Manna, L. Aging of Self-Assembled Lead Halide Perovskite Nanocrystal Superlattices: Effects on Photoluminescence and Energy Transfer. *ACS Nano* **2021**, *15* (1), 650−664.

https://doi.org/10.1021/jacs.3c12723
J. Am. Chem. Soc. 2024, 146, 8189−8197